Article

Nanoparticle Air Filtration Using MXene-Coated Textiles

Prastuti Upadhyay [1], Stefano Ippolito [1], Bita Soltan Mohammadlou [1,2], Michael S. Waring [3] and Yury Gogotsi [1,*]

[1] A. J. Drexel Nanomaterials Institute and Department of Materials Science and Engineering, Drexel University, 3141 Chestnut Street, Philadelphia, PA 19104, USA; pu34@drexel.edu (P.U.); si368@drexel.edu (S.I.); bs3298@drexel.edu (B.S.M.)

[2] Department of Mechanical Engineering and Mechanics, Drexel University, 3141 Chestnut Street, Philadelphia, PA 19104, USA

[3] Department of Civil, Architectural and Environmental Engineering, Drexel University, 3141 Chestnut Street, Philadelphia, PA 19104, USA; msw59@drexel.edu

* Correspondence: gogotsi@drexel.edu

Abstract: Nanoparticles with aerodynamic diameters of less than 100 nm pose serious problems to human health due to their small size and large surface area. Despite continuous progress in materials science to develop air remediation technologies, efficient nanoparticle filtration has appeared to be challenging. This study showcases the great promise of MXene-coated polyester textiles to efficiently filter nanoparticles, achieving a high efficiency of ~90% within the 15–30 nm range. Using alkaline earth metal ions to assist textile coating drastically improves the filter performance by ca. 25%, with the structure–property relationship thoroughly assessed by electron microscopy and X-ray computed tomography. Such techniques confirm metal ions' crucial role in obtaining fully coated and impregnated textiles, which increases tortuosity and structural features that boost the ultimate filtration efficiency. Our work provides a novel perspective on using MXene textiles for nanoparticle filtration, presenting a viable alternative to produce high-performance air filters for real-world applications.

Keywords: MXenes; coatings; textiles; air filtration; nanoparticles

1. Introduction

Since their discovery in 2011, MXenes—the largest family of two-dimensional (2D) materials—have been explored in many applications, including electronics, electromagnetic interference shielding, energy storage, catalysis, sensing, and biomedicine [1]. MXenes have the general formula $M_{n+1}X_nT_x$, where M represents an early transition metal, X is carbon and/or nitrogen, T_x describes the surface terminations (mostly -O, -OH, -F, and -Cl), and *n* ranges from 1 to 4 [2]. Such 2D materials are synthesized from their bulk MAX phase precursors via wet chemical etching and delamination protocols. MXenes have unique and versatile properties, such as metallic electrical conductivity, tunable electrochemical and plasmonic properties, active redox surface, and high hydrophilicity [3]. Moreover, the synthesis of MXenes is not only limited to small-scale synthesis; it can be expanded to large-scale industrial applications capitalizing on established technologies using HF and HCl, like in petroleum, and to semiconductor manufacturing industries, with best practices as highlighted in the literature [4,5].

Over the last few years, the adsorption capacity of MXenes has been investigated for gasses like CO_2 [6], CH_4 [7], and H_2 and toxic species such as NO, CO, NO_2, NH_3, SO_2, and H_2S, as well as different volatile organic compounds [8]. Besides their gas adsorption

properties, MXenes have been explored for viral aerosol removal [9] and $PM_{2.5}$ filtration (particulate matter with an aerodynamic diameter smaller than 2.5 μm) using polyacrylonitrile [10] and Nylon filters [11]. Despite a steady increase of ~10% in MXene-related studies for environmental applications during 2018–2022 [12], works on MXenes for air filtration appear sparse, only covering ~0.2% of the MXene literature. Still, there is an agreement that MXenes show promise in air filtration and air quality control applications [13–15].

Here, we reported an unprecedented study using Ti_3C_2 MXene-coated textiles as air filters for nanoparticles (NPs) with aerodynamic diameters smaller than 100 nm. Such NPs are commonly produced in urban areas as a result of vehicular traffic and industrial emissions [16,17], posing a serious threat to human health due to the increased risk of developing respiratory and cardiovascular diseases [18,19], as well as neurological disorders [20]. We developed a straightforward approach to producing Ti_3C_2-coated polyester textiles as air filters, targeting NPs with sizes below 100 nm. Using metal ions to assist with the MXene coating led to different morphological characteristics, as confirmed by electron microscopy and X-ray tomography, thereby improving the ultimate filtration efficiency, reaching ~90% in the 15–30 nm range. We also speculate that our systems could behave like self-cleaning filters, taking advantage of Joule heating and, therefore, exploiting the metallic conductivity of MXenes and their thermal properties.

2. Materials and Methods

2.1. Synthesis of Ti_3C_2 MXene

Ti_3C_2 MXene was synthesized by wet chemical etching, starting from the Ti_3AlC_2 MAX precursor (Carbon-Ukraine, Kyiv, Ukraine) via the conventional HF/HCl method and using LiCl as a delaminating agent, in agreement with the previously reported literature [21]. For 1 g of MAX phase, 6 mL of deionized (DI) water, 12 mL of 12 M HCl (Fisher Scientific, Bridgewater, NJ, USA), and 2 mL of 50 wt.% HF (Acros Organics, Bridgewater, NJ, USA) were used to prepare the etching solution, which was kept under stirring at 300 rpm and 35 °C for 24 h. Then, the dispersion was neutralized using DI water and multiple centrifugation steps at 3500 rpm for 5 min. After neutral pH was reached, multilayer Ti_3C_2 was delaminated using 1 g of LiCl (anhydrous ≥ 98%, Alfa Aesar, Ward Hill, MA, USA) in 50 mL of DI water at 35 °C for 24 h. Later, LiCl was removed via multiple centrifugation steps at 3500 rpm for 15 min until a dark supernatant was obtained. The single-layer Ti_3C_2 flakes were collected, and the dispersion was concentrated to 10 mg/mL. This MXene is hydrophilic and negatively charged in solution due to its O, OH and F surface terminations (T_x). Its formula is often written as $Ti_3C_2T_x$, but we omit T for simplicity, as only one kind of MXene was used.

2.2. Fabrication of Ti_3C_2- and Ti_3C_2/Mg(II)-Coated Textile

Hydrophilic MXenes strongly adhere to the fibers when coated on textiles, providing excellent coatings over various substrates. First, we conducted a parametric study to select the best concentration of Ti_3C_2 dispersion to be used to maximize the MXene loading on the textile. We used non-woven polyester textile due to its low cost and lower filtration efficiency compared to high-efficiency air filters for particulate matter below 0.3 μm. Small polyester pieces (2.5 × 2.5 cm^2) were dip-coated using 1, 5, 10, 15, and 20 mg/mL Ti_3C_2 aqueous dispersion, soaking them for 5 min on each side. Then, the coated textiles were freeze-dried for 2 days (Labconco Freezone 2.5 plus Freeze Dryer, at −85 °C at 0.10 mbar). Once completely dried, we compared the mass of the fabric pieces before and after coating, recording the highest loading for the MXene dispersion with a concentration equal to 10 mg/mL, then selected for the following investigations and sample preparation steps [Figure S1a]. We attribute the highest loading for 10 mg/mL MXene dispersion to its optimal rheological property,

leading to the best impregnation of the textile fibers during the coating process. To further improve the loading on textiles and their impregnation, we developed a protocol based on metal ion-assisted coating using Mg-ions (henceforth $Ti_3C_2/Mg(II)$) contained in a $MgCl_2$ aqueous solution where, after soaking the textile in MXene dispersion, we also soaked it in Mg (II) solution before drying it for 15 min. By favoring the MXene–MXene and MXene–fiber electrostatic interaction [22], this additional step improves the quality of coating as well as the overall loading on the textile [Figure S1a].

At this point, for the filtration analysis, two different kinds of sample types were prepared: (i) Ti_3C_2-coated [Figure 1a] and (ii) $Ti_3C_2/Mg(II)$-coated textiles [Figure 1b]. All samples were prepared starting from uncoated textiles (15×15 cm^2) and using Ti_3C_2 dispersion at 10 mg/mL. In addition, the 0.5 M aqueous solution of $MgCl_2$ was used for sample (ii), following identical steps to those reported above for the parametric study.
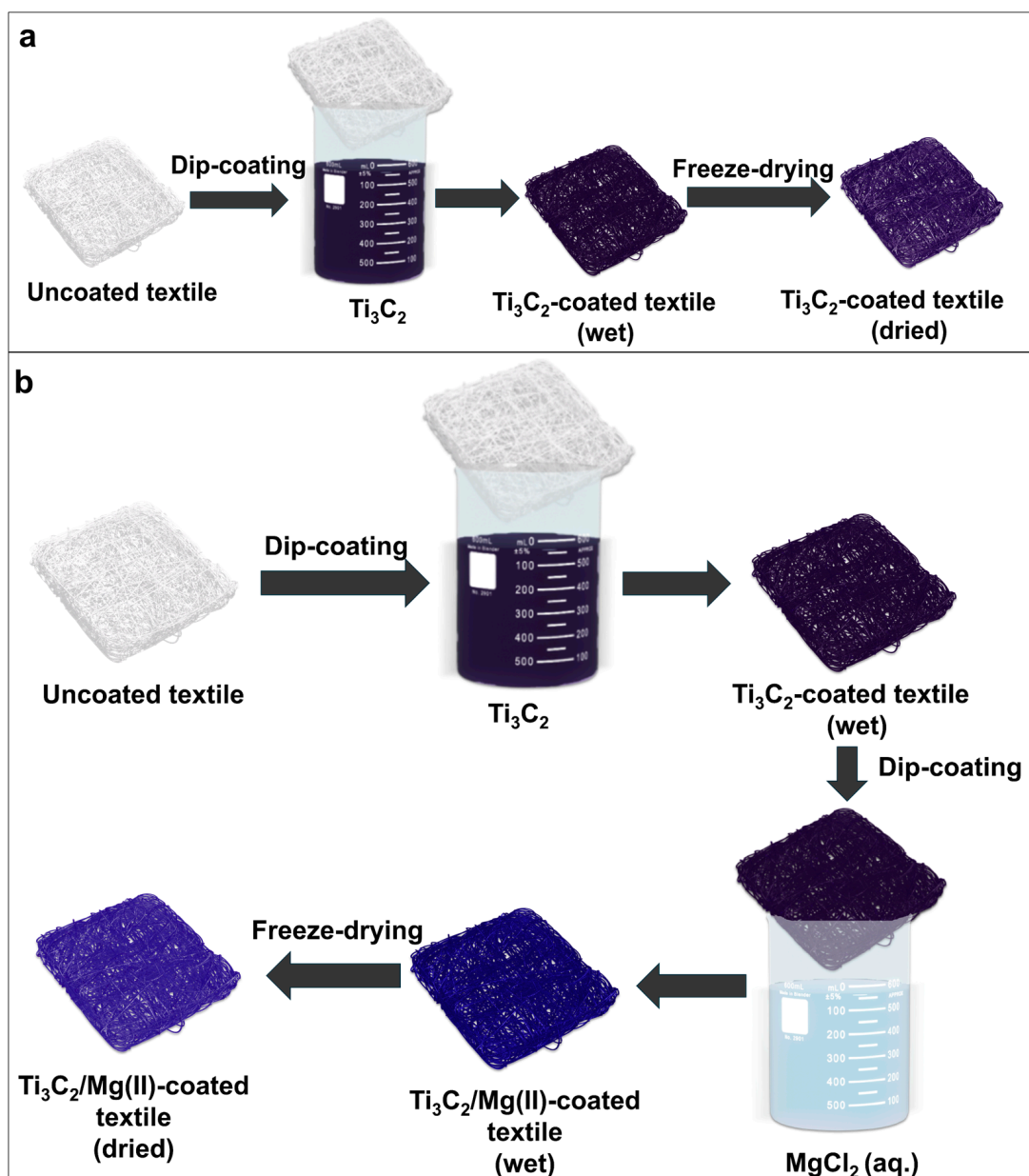

Figure 1. Schematic illustration for the production of (**a**) Ti_3C_2- and (**b**) $Ti_3C_2/Mg(II)$-coated textile air filters.

2.3. Multiscale Characterization of the Fabrics

The multiscale characterization of the coated textile was performed using the following techniques.

2.3.1. Scanning Electron Microscopy/Electron Dispersive X-Ray Spectroscopy (SEM/EDS)

The textiles were analyzed using a Zeiss Supra 50 VP microscope operating at 10 kV. The same SEM instrument was used for EDS investigations. Each spectrum was collected at 10 kV, and three spots were collected at different locations for each sample. In all cases, the recorded spectra contained more than 50,000 counts.

2.3.2. Micro-Computed Tomography (Micro-CT)

Micro-CT investigations were conducted using the Zeiss Xradia 620 Versa, performing two sets of resolution scans to analyze coated textiles for air filtration applications. The first set of scans was conducted on coated textiles at 50 kV using a 4X objective, resulting in a pixel size of 2.12 μm. Additional information on the second set of scans is included in Figure S3. All scans were performed in the air at ambient temperature, capturing 2401 projection images for each dataset.

The micro-CT data were reconstructed using Zeiss XRM Reconstructor software (Version 16.5.13718.44212) to produce precise 3D volumetric datasets. Post-processing was performed with ORS Dragonfly Pro software (Version 2022.2.0.1367), focusing on qualitative and quantitative analysis to study the distribution of MXene coatings. This detailed investigation provided valuable information for assessing fabrication quality and textile coating differences for air filtration applications.

2.3.3. Efficiency Testing System

In the filtration setup the sodium chloride (NaCl) aerosol was emitted into a vacuum-sealed chamber from a generation system consisting of a pump, filter, atomizer (TSI 3076), diffusion dryer (TSI 3062), and (TSI 3077A). In the system, aerosols are charged positively using a corona charger such that electron mobility is induced due to repulsion with a positively charged electrode in the instrument. Each filter was clamped inside the chamber between two torus-shaped clamps, where only the coated area was exposed to the aerosol. The aerosol concentration, in terms of time and size-resolved particle number, was measured in variable size diameters from 5.6 nm to 560 nm using the Fast Mobility Particle Sizer (TSI FMPS 3091). In all, 108 sets of data were collected during each testing cycle. The filtration efficiency (η) was calculated using the ratio of the concentration of aerosol passing through the filter (C_1) over the concentration of the aerosol in the chamber (C_0), following Equation (1) [23]:

$$\eta = \left(1 - \frac{C_1}{C_0} \right) \times 100\% \tag{1}$$

Data treatment and statistical analysis were performed using OriginPro software (Version 2023).

3. Results and Discussion

3.1. Morphological Characterization

The SEM and EDS analysis of uncoated [Figure 2a] and coated textiles provided valuable insights into the sample morphology and homogeneity. Ti_3C_2-coated filters presented 2D flakes covering the randomly oriented polyester fibers [Figure 2b], showing no major differences compared to Ti_3C_2/Mg(II)-coated textiles [Figure 2c]. In this regard, we mapped the spatial elemental composition and distribution of the two different samples by looking at carbon, titanium, fluorine, chlorine, oxygen, and magnesium spectra [Figure 2d]. The

EDS data confirmed uniform elemental distribution and high sample homogeneity in both kinds of textiles, which, combined with the SEM results, provided unambiguous evidence about the similar surface morphology for both samples. In addition, our morphological characterization demonstrated that any difference in filtration efficiency for the two systems under investigation could not be due to surface effects in the filters but rather to internal structural features.
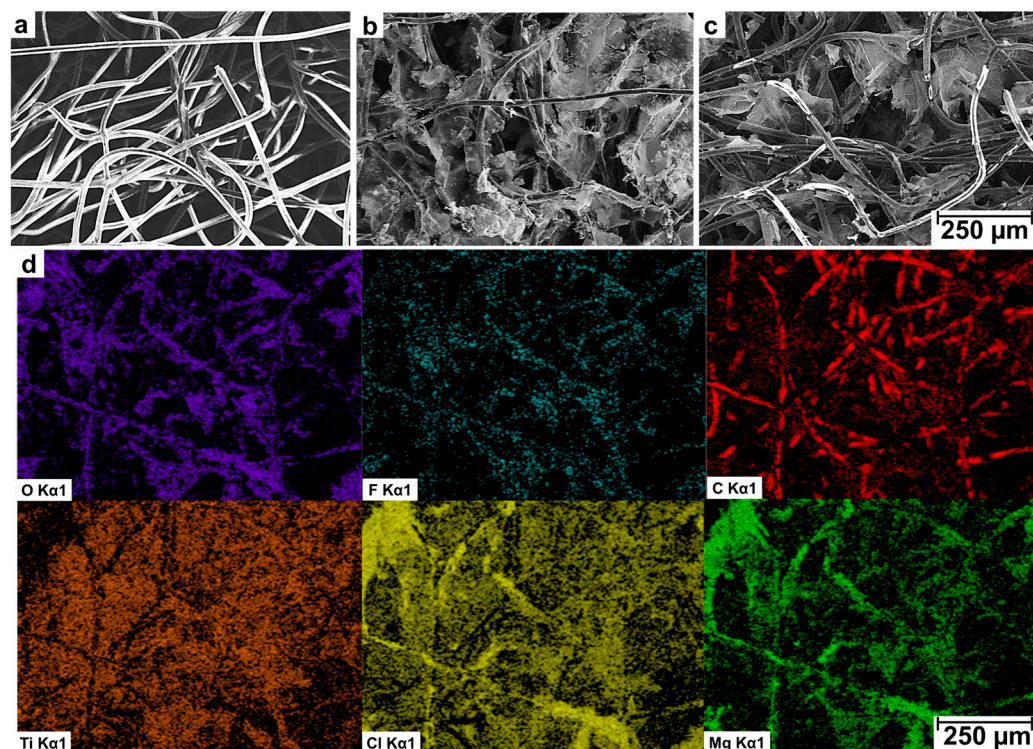

Figure 2. Scanning electron microscopy images of (**a**) uncoated textile, (**b**) Ti_3C_2-coated textile, (**c**) Ti_3C_2/Mg (II)-coated textile. (**d**) Elemental mappings collected on Ti_3C_2/Mg (II)-coated textile.

3.2. Structural Analysis

Following SEM and EDS characterization, we thoroughly investigated the internal structural features of Ti_3C_2- and Ti_3C_2/Mg(II)-coated textiles using Micro-CT. Excellent adherence and coverage throughout the substrate were observed for both systems. As shown in the 2D cross-sectional images from Micro-CT, the Ti_3C_2-coated textiles [Figure 3a,b] exhibited randomly scattered and sparsely distributed MXene flakes covering the fibers. In contrast, the Ti_3C_2/Mg(II)-coated samples [Figure 3c,d] displayed a denser and more uniform coating, with a higher degree of MXene aggregation around the textile fibers. This suggests that adding Mg(II) enhances MXene distribution during the coating process, potentially improving the filtration performance of these systems. Such structural characteristics were further visualized through 3D Micro-CT images for both Ti_3C_2-coated textiles [Figure 3e,f] and the denser Ti_3C_2/Mg(II) samples [Figure 3g,h]. To complement these qualitative 3D visualizations, the samples' porosity and the loaded MXene volume were also quantified. Ti_3C_2-coated textiles demonstrated an average porosity of about ~70%, while the Ti_3C_2/Mg(II)-coated samples exhibited a slightly lower porosity of approximately 65%. The reduced porosity indicates higher MXene loading in Ti_3C_2/Mg(II)-coated samples, leading to a denser coating, which aligns with the data collected during the parametric study. This reduction in porosity (viz., higher loading) and the improved MXene distribution within the filter highlight an enhanced geometric tortuosity in our air filters, a figure of merit strongly influencing their filtration efficiency [24].
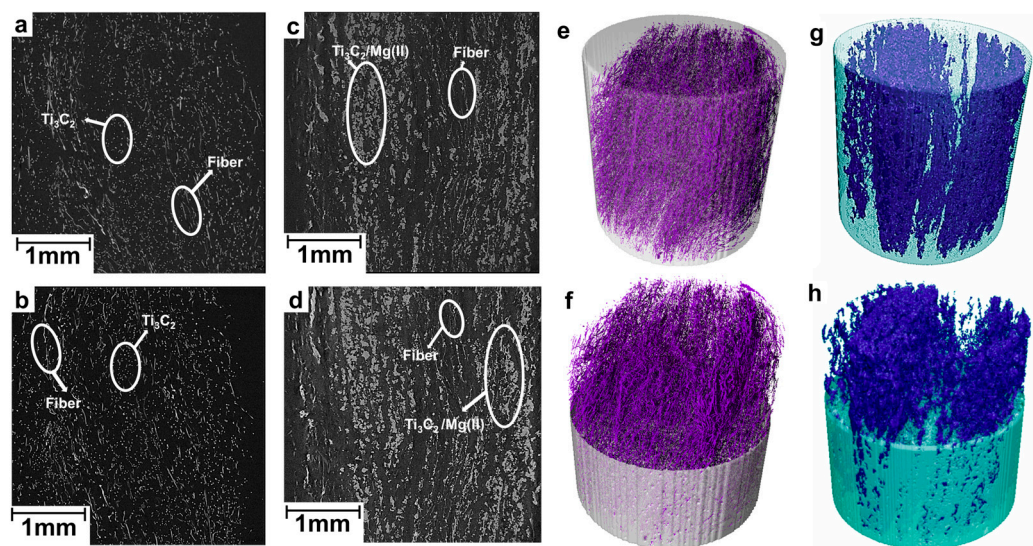
Figure 3. (**a**,**b**) Typical 2D cross-sectional Micro-CT images of Ti_3C_2-coated textile (MXene: gray; textile: fibrous lines). (**c**,**d**) Typical 2D cross-sectional Micro-CT images of $Ti_3C_2/Mg(II)$-coated textile (MXene/Mg(II): gray; textile: fibrous lines). (**e**,**f**) Three-dimensional Micro-CT images of Ti_3C_2-coated textile in unit space (gray). (**g**,**h**) Three-dimensional Micro-CT image of $Ti_3C_2/Mg(II)$-coated textile in unit space (green).

3.3. Filtration Efficiency

We assessed the filtration efficiency (η) of three different types of samples: (i) uncoated polyester textile, (ii) Ti_3C_2-coated textile, and (iii) $Ti_3C_2/Mg(II)$-coated textile. To this end, we calculated η (Equation (1)) by using the data collected with a fast mobility particle sizer (FMPS), measuring the concentration ratio between the NaCl aerosol passing through the filter (C_1) and the NaCl aerosol in the chamber air (C_0), targeting particle sizes ranging from 5.6 nm to 560 nm. The $Ti_3C_2/Mg(II)$-coated samples significantly outperformed the other two sample types, reaching $\eta \approx 90\%$ in the 15–30 nm range [Figure 4b]. A similar trend was also observed in the other size ranges, such as 30–60 nm, 60–120 nm, 120–250 nm, and 250–560 nm, where the $Ti_3C_2/Mg(II)$ samples performed as the best filters, followed by the Ti_3C_2-coated and uncoated textiles. The enhanced performance of $Ti_3C_2/Mg(II)$-coated textiles could be likely linked to the resulting decrease in porosity as confirmed by micro-CT investigations, which not only reduced pore sizes but increased the tortuosity of the filter medium. In addition to their morphological and structural characteristics, improved geometric tortuosity creates complex pathways for better particle capture, leading to higher filtration efficiency. Finally, charged polar surfaces of MXenes may contribute to the capture of nanoparticles. This agrees with the results collected by SEM and micro-CT investigations, which showed that the MXene flake could cover the polyester fibers differently, depending on the production steps. In particular, using metal ions to assist the coating enhanced the geometric tortuosity within the filters, as pointed out by the higher MXene loading and the better aggregation of flakes around the fibers. In addition, a possible contribution of electrostatic interaction cannot be ruled out, as the presence of metal ions within the filter structure could improve filtration efficiency, further supporting the data collected.
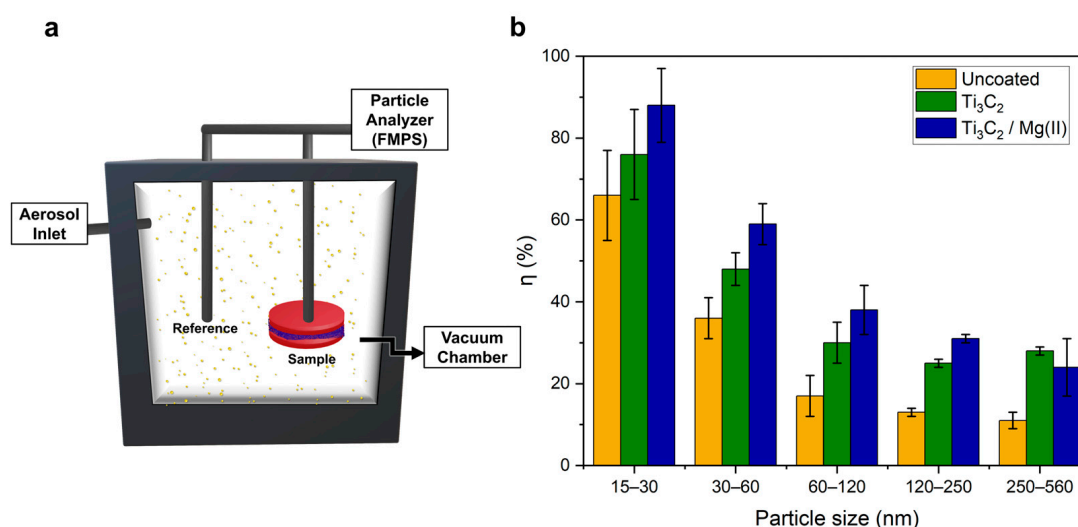
Figure 4. (**a**) A schematic of the filtration testing setup, where the samples are sandwiched between two red clamps inside a vacuum chamber (bottom). Then, this is filled with an aerosol of NaCl particles entering from the aerosol inlet (left), and data are collected by a particle analyzer (FMPS, right). (**b**) The filtration efficiency (η) of the NaCl aerosol for the uncoated textile and Ti_3C_2-and $Ti_3C_2/Mg(II)$-coated textile within a particle range from 5.6 nm to 560 nm.

Moreover, taking advantage of the unique and versatile MXene properties, including high hydrophilicity and metallic conductivity, we speculate about the possibility of producing high-efficiency and self-cleaning filters for gas and virus filtration. The latter applications rely on systems with high filtration efficiency in the particle range considered in our study. As displayed in Figure S5b, we tested the Joule heating of our MXene-coated filters, reaching a temperature above 100 °C while applying a voltage bias of less than 15 V. In particular, $Ti_3C_2/Mg(II)$-coated textiles presented a less abrupt temperature rise [Figure S5a], which could allow for a better fine-tuning of the temperature needed to clean and thus regenerate the filter, thereby providing additional value to our work. We expect our findings to stimulate additional research on using MXene textiles as air filters, further expanding the range of applications of such a unique family of 2D materials.

4. Conclusions

In conclusion, we tested the air filtration efficiency of MXene-coated polyester textiles and demonstrated superior performance for samples prepared through metal ion-assisted coating. This enhanced efficiency results from the higher and better loading of MXene flakes within the textile fibers, as confirmed by morphological and structural analyses performed via SEM and Micro-CT. We reached an efficiency close to 90% for NPs in the 15–30 nm range, achieving state-of-the-art performance using a straightforward, fast, and environmentally friendly sample preparation protocol. While such results are encouraging regarding the use of MXene-coated textiles for real-world applications concerning air filtration, it is worth mentioning that our air filters could still be improved in future studies focused on the optimization of the MXene structure, nature, and concentration of metal ions, as well as the suitable choice of substrate to coat.

textile at 10 mg/mL. The scale bar is 125 μm. Figure S3: (a,b) Two-dimensional cross-sectional micro-CT images showing uncoated textiles (fibrous lines). (c,d) Two-dimensional cross-sectional micro-CT images of Ti_3C_2-coated textile, showing Ti_3C_2 flake aggregations (gray) and textile (fibrous lines). (e,f) Cross-sectional Micro-CT images of Ti_3C_2/Mg (II)-coated textile, showing $Ti_3C_2/Mg(II)$ flake aggregations (gray) and textile (fibrous lines). Figure S4: Comparison of filtration efficiency for 1-layer and 5-layer uncoated textiles. Figure S5: (a) Temperature increases with increasing voltage bias for Ti_3C_2-coated textile (green) and $Ti_3C_2/Mg(II)$-coated textile (blue). (b) Experimental setup for the Joule heating testing. (c) Picture collected by infrared camera showing Joule heating in $Ti_3C_2/Mg(II)$-coated samples. Figure S6: Schematics show the possible regeneration mechanism via Joule heating for Ti_3C_2-coated textiles for air purification (e.g., nanoparticle filtration). Refs. [25,26] are cited in Supplementary Materials file.

Author Contributions: Conceptualization, P.U. and S.I.; data curation, P.U. and S.I.; formal analysis, P.U. and B.S.M.; funding acquisition, Y.G.; investigation, P.U. and S.I.; methodology, P.U., S.I. and M.S.W.; project administration, P.U. and S.I.; resources, M.S.W. and Y.G.; visualization, P.U. and B.S.M.; writing—original draft, P.U. and S.I.; writing—review and editing, P.U., S.I., B.S.M., M.S.W. and Y.G. All authors have read and agreed to the published version of the manuscript.

Data Availability Statement: The data supporting the conclusions of this article are available on request from the corresponding author.

Conflicts of Interest: The authors declare no conflicts of interest.

References

1. Gogotsi, Y.; Anasori, B. The Rise of MXenes. *ACS Nano* **2019**, *13*, 8491–8494. [CrossRef] [PubMed]

2. Naguib, M.; Kurtoglu, M.; Presser, V.; Lu, J.; Niu, J.; Heon, M.; Hultman, L.; Gogotsi, Y.; Barsoum, M.W. Two-Dimensional Nanocrystals Produced by Exfoliation of Ti_3AlC_2. *Adv. Mater.* **2011**, *23*, 4248–4253. [CrossRef] [PubMed]

3. VahidMohammadi, A.; Rosen, J.; Gogotsi, Y. The World of Two-Dimensional Carbides and Nitrides (MXenes). *Science* **2021**, *372*, eabf1581. [CrossRef] [PubMed]

4. Shuck, C.E.; Ventura-Martinez, K.; Goad, A.; Uzun, S.; Shekhirev, M.; Gogotsi, Y. Safe Synthesis of MAX and MXene: Guidelines to Reduce Risk During Synthesis. *ACS Chem. Health Saf.* **2021**, *28*, 326–338. [CrossRef]

5. Downes, M.; Shuck, C.E.; McBride, B.; Busa, J.; Gogotsi, Y. Comprehensive Synthesis of $Ti_3C_2T_x$ from MAX Phase to MXene. *Nat. Protoc.* **2024**, *19*, 1807–1834. [CrossRef] [PubMed]

6. Morales-García, Á.; Fernández-Fernández, A.; Viñes, F.; Illas, F. CO_2 Abatement Using Two-Dimensional MXene Carbides. *J. Mater. Chem. A* **2018**, *6*, 3381–3385. [CrossRef]

7. Liu, F.; Zhou, A.; Chen, J.; Jia, J.; Zhou, W.; Wang, L.; Hu, Q. Preparation of Ti_3C_2 and Ti_2C MXenes by Fluoride Salts Etching and Methane Adsorptive Properties. *Appl. Surf. Sci.* **2017**, *416*, 781–789. [CrossRef]

8. Yuan, W.; Yang, K.; Peng, H.; Li, F.; Yin, F. A Flexible VOCs Sensor Based on a 3D MXene Framework with a High Sensing Performance. *J. Mater. Chem. A* **2018**, *6*, 18116–18124. [CrossRef]

9. Liu, F.; Ma, Q.; Sabuj, M.M.A.; Yen, S.-H.; Govindan, D.; Gao, J.; Zhao, M.; Elimelech, M.; Zhang, W. Revolutionizing Airborne Virus Defense: Electromagnetic MXene-Coated Air Filtration for Superior Aerosol Viral Removal. *ACS Appl. Mater. Interfaces* **2024**, *16*, 10148–10157. [CrossRef]

10. Gao, X.; Li, Z.-K.; Xue, J.; Qian, Y.; Zhang, L.-Z.; Caro, J.; Wang, H. Titanium Carbide $Ti_3C_2T_x$ (MXene) Enhanced PAN Nanofiber Membrane for Air Purification. *J. Membr. Sci.* **2019**, *586*, 162–169. [CrossRef]

11. Baskoy, M.H.; Cetin, O.; Koylan, S.; Khan, Y.; Tuncel, G.; Erguder, T.H.; Unalan, H.E. MXene-Decorated Nylon Mesh Filters for Improvement of Indoor Air Quality by $PM_{2.5}$ Filtration. *ACS Omega* **2023**, *8*, 23465–23476. [CrossRef] [PubMed]

12. Georgantas, Y.; Moissinac, F.P.; Bissett, M. MXenes-Mining: A Decade of Discovery. *Graphene 2D Mater.* **2024**, *9*, 5–26. [CrossRef]

13. Dixit, F.; Zimmermann, K.; Alamoudi, M.; Abkar, L.; Barbeau, B.; Mohseni, M.; Kandasubramanian, B.; Smith, K. Application of MXenes for Air Purification, Gas Separation and Storage: A Review. *Renew. Sustain. Energy Rev.* **2022**, *164*, 112527. [CrossRef]

14. Kim, J.T.; Lee, C.W.; Jung, H.J.; Choi, H.J.; Salman, A.; Padmajan Sasikala, S.; Kim, S.O. Application of 2D Materials for Adsorptive Removal of Air Pollutants. *ACS Nano* **2022**, *16*, 17687–17707. [CrossRef]

15. Niu, C.; Yang, L.; Sun, H.; Zhu, Z.; Liang, W.; Li, J.; Li, A. Holey Ti3C2Tx Nanosheets Membrane with High PM Removal Efficiency for Air Pollution. *J. Environ. Chem. Eng.* **2023**, *11*, 111113. [CrossRef]

16. Kumar, P.; Morawska, L.; Birmili, W.; Paasonen, P.; Hu, M.; Kulmala, M.; Harrison, R.M.; Norford, L.; Britter, R. Ultrafine Particles in Cities. *Environ. Int.* **2014**, *66*, 1–10. [CrossRef]

17. Moreno-Ríos, A.L.; Tejeda-Benítez, L.P.; Bustillo-Lecompte, C.F. Sources, Characteristics, Toxicity, and Control of Ultrafine Particles: An Overview. *Geosci. Front.* **2022**, *13*, 101147. [CrossRef]

18. Münzel, T.; Hahad, O.; Daiber, A.; Lelieveld, J. Luftverschmutzung und Herz-Kreislauf-Erkrankungen. *Herz* **2021**, *46*, 120–128. [CrossRef] [PubMed]

19. Ohlwein, S.; Kappeler, R.; Kutlar Joss, M.; Künzli, N.; Hoffmann, B. Health Effects of Ultrafine Particles: A Systematic Literature Review Update of Epidemiological Evidence. *Int. J. Public Health* **2019**, *64*, 547–559. [CrossRef]

20. Flood-Garibay, J.A.; Angulo-Molina, A.; Méndez-Rojas, M.Á. Particulate Matter and Ultrafine Particles in Urban Air Pollution and Their Effect on the Nervous System. *Environ. Sci. Process. Impacts* **2023**, *25*, 704–726. [CrossRef]

21. Mathis, T.S.; Maleski, K.; Goad, A.; Sarycheva, A.; Anayee, M.; Foucher, A.C.; Hantanasirisakul, K.; Shuck, C.E.; Stach, E.A.; Gogotsi, Y. Modified MAX Phase Synthesis for Environmentally Stable and Highly Conductive Ti$_3$C$_2$ MXene. *ACS Nano* **2021**, *15*, 6420–6429. [CrossRef] [PubMed]

22. Deng, Y.; Shang, T.; Wu, Z.; Tao, Y.; Luo, C.; Liang, J.; Han, D.; Lyu, R.; Qi, C.; Lv, W.; et al. Fast Gelation of Ti$_3$C$_2$T$_x$ MXene Initiated by Metal Ions. *Adv. Mater.* **2019**, *31*, 1902432. [CrossRef] [PubMed]

23. Fujiwara, Y.; Goto, M.; Iigaki, K.; Iyoku, T.; Quan Ho, H.; Kawamoto, T.; Kondo, M.; Kunitomi, K.; Morita, K.; Nagasumi, S.; et al. Design of High Temperature Engineering Test Reactor (HTTR). In *High Temperature Gas-Cooled Reactors*; Takeda, T., Inagaki, Y., Eds.; JSME Series in Thermal and Nuclear Power Generation; Academic Press: Cambridge, MA, USA, 2021; Volume 5, pp. 17–177, ISBN 978-0-12-821031-4.

24. Ávila, J.; Pagalo, J.; Espinoza-Andaluz, M. Evaluation of Geometric Tortuosity for 3D Digitally Generated Porous Media Considering the Pore Size Distribution and the A-Star Algorithm. *Sci. Rep.* **2022**, *12*, 19463. [CrossRef] [PubMed]

25. David, E.; Niculescu, V.-C. Volatile Organic Compounds (VOCs) as Environmental Pollutants: Occurrence and Mitigation Using Nanomaterials. *Int. J. Environ. Res. Public Health* **2021**, *18*, 13147. [CrossRef] [PubMed]

26. Aromaa, J.; Kekkonen, M.; Mousapour, M.; Jokilaakso, A.; Lundström, M. The Oxidation of Copper in Air at Temperatures up to 100 °C. *Corros. Mater. Degrad.* **2021**, *2*, 625–640. [CrossRef]